CH$_4$ fragmentation from single and double ionization by proton and electron impact

H. Luna,[*] W. Wolff,[†] and E. C. Montenegro[‡]

Universidade Federal do Rio de Janeiro (UFRJ), 21941-972 Rio de Janeiro, RJ, Brazil

L. Sigaud[§]

Universidade Federal Fluminense, 24210-346 Niteroi, RJ, Brazil

The fragmentation of methane by impact of electrons and protons is studied experimentally to reveal the mechanisms behind fragmentation by projectiles with opposite charges. Coincidence measurements are used to separate the single from double ionization, in the case of protons, and the DETOF (delayed extraction time-of-flight) technique is used, in the case of electrons, to untangle kinematic signatures of the single vacancy from that of the one-electron–two-vacancy satellite states populated during the collision. The substantial differences in the fragmentation cross sections observed between the two projectiles, when several hydrogen bonds are broken, are here attributed essentially to single ionization and interpreted as due to the interference term between the mechanisms of shakeup and the excitation ionization by double impact that appears in the perturbative expansion of the ionization cross section.

I. INTRODUCTION

The fragmentation of molecules by ionizing particles is a rather complex phenomenon that may involve the simultaneous breaking of several chemical bonds with the consequent ejection of several highly reactive products. These products influence the inventory of a large number of physicochemical environments subjected to radiation, as diverse as planetary atmospheres, magnetospheres, or the human body under radiation therapy. The ejection of a larger number of fragments occurs preferentially if the removed electron comes from the innermost shell of the heavier nuclei or the inner valence orbitals of the molecule. The rapid electronic rearrangement, strongly influenced by the electron-electron correlations, makes the fragmentation process a mosaic of details that turn its description into a great theoretical challenge that has been faced for decades. Due to its strong symmetry and ease of handling in the laboratory, methane has been widely used, both theoretically and experimentally, to explore many of the key issues behind many-body fragmentation processes.

The study of ionization and molecular fragmentation of methane by charged particle impact dates back to 1924. That year, Hughes and Klein [1] were able to obtain the methane ionization curve by electrons from 14 to 300 eV, having first observed the now well-known shape of the ionization cross section. About a decade later, Hipple and Bleakney [2] used a mass spectrometer to determine the appearance potentials of the various CH$_4$ fragments that are ejected due to electron impact ionization. Shortly after, Smith [3] listed the various possible fragmentation channels associated with the ejected ionic fragments CH$_4^+$, CH$_3^+$, CH$_2^+$, CH$^+$, C$^+$, H$_2^+$, and H$^+$, measuring their appearance potentials and relative yields in an attempt to connect their appearance potentials to the different energy levels of methane molecular orbitals. At this point, it became clear that such an association is not straightforward in the case of many-body fragmentation. Indeed, the appearance potentials are related to four quantities: the dissociation energy, the ionization energy, and the excitation and kinetic energies of the ejected products. In the common case where some of the products are neutral, their kinetic energies are difficult to be measured or theoretically estimated. This scenario hinders a comprehensive view of the energy balance of the multifragmentation process to this day.

The way the redistribution of the energy delivered by the projectile occurs in a molecule is a conceptually basic matter and of great practical interest. Recent efforts have been made to better quantify the energy balance by measuring the kinetic energy distribution (KED) of the fragments [4–9]. However, some ambiguities remain, since some competing fragmentation channels, such as CH$_2^+$ + 2H and CH$_2^+$ + H$_2$, or different initial states, for example, those associated to vertical transitions or satellite states, can leave indistinguishable signatures in the KED. This is a key issue addressed in this paper.

The available energy to be redistributed is strongly associated with the molecular orbital in which the primary vacancy is created by the projectile. Thus, a first step to identify the fragmentation pathways chosen by the molecule is to relate the yields of the various ejected fragments to the molecular orbitals where the primary vacancies are created. Backx and Van der Wiel [10] took advantage of the small number of molecular orbitals of CH_4, whose ground-state electronic configuration is $(1a_1)^2(2a_1)^2(1t_2)^6$, to relate the

[*]hluna@if.ufrj.br

[†]wania@if.ufrj.br

[‡]montenegro@if.ufrj.br

[§]lsigaud@if.uff.br

branching ratios for CH_4^+, CH_3^+, CH_2^+, CH^+, and H^+ production with the $(2a_1)^{-1}$ and $(1t_2)^{-1}$ vacancies created from vertical transitions induced by 10-keV electron impact. However, this association is not at all comprehensive because it does not include the significant contribution, found by those authors, of one-electron–two-vacancy satellite or shake-up states, with energies near that of $(2a_1)^{-1}$. These shake-up states, appearing in a wide variety of molecules [11,12], have been identified in methane through electron momentum spectroscopy [13,14], photoionization [15,16], and electron impact fragmentation [17], and originate from the strong influence of electron-electron correlation during relaxation following the production of a vacancy in an inner valence orbital. For electron impact, it was shown that the contribution due to satellite states increases in importance as the number of moieties increases, with C^+ being originated almost exclusively from satellite states [17]. This increasing role of satellite states in the fragmentation channels resulting in a larger number of moieties seems to be more universal than regarded so far, as the same conclusion was reached recently for the production of O^+ from water, also by electron impact [18].

For swift projectiles, when the collision time is much shorter than the relaxation time, the branching ratios of the ejected fragments associated with the various molecular orbitals can be considered as a characteristic of the molecule that does not depend on the velocity of the projectile. In turn, the velocity and type of the projectile determine the population of primary vacancies produced in the various molecular orbitals and, ultimately, the yields of the observed fragments. Thus, the fragmentation process can be separated into two steps: the production of primary vacancies by the projectile and the relaxation of the molecules with its subsequent fragmentation. Both steps are quite complex to describe theoretically due to the multicenter character of the system, the strong role of the electron-electron correlation, and the vibrational coupling that breaks down the independent electron and the Born-Oppenheimer approximations.

In this scenario, additional information related to the dynamic behavior of the entire process, based on the knowledge of the values and shape of the fragment-ion-production cross section as a function of the projectile velocity, is required. Fragment-ion cross-section measurements have been performed in methane by several authors over the last decades, mainly for electron [19–24] and proton [25–28] impact, for a wide range of velocities.

Due to the difficulty of theoretically treating the ionization of multielectronic and multicentric systems, few attempts have been made so far to associate the values and shape of the observed fragment-ion with the single- and double-ionization cross sections [29–31]. These studies were made for the proton case and use the semiempirical decay model proposed by Luna *et al.* [28], which goes over the details of the production and relaxation process of the vacancies created in the molecular orbitals to directly relate the observed to the calculated sets of cross sections [29,31]. This approach, while useful for evaluating the quality of ionization cross-section calculations, hides important details of the energy redistribution process, which starts with either the vertical transitions or satellite states.

For the case of electron impact, Liu and Shemansky [17] were able to determine the contributions from the single vacancy (vertical transitions) and from one-electron–two-vacancy satellite or shake-up states to the fragment-ion cross sections, adjusting the measured cross sections using a sum of semiempirical expressions that describe the behavior of these two contributions as a function of the impact energy. This adjustment shows, as already mentioned, that C^+ is almost exclusively originated from satellite states. This conclusion is in agreement with the results obtained by Samson *et al.* [15] in the case of photofragmentation, but stronger experimental indications for the case of electron impact were still missing. In this work a clear experimental signature of the vertical and satellite contributions to fragmentation is uncovered via the distribution of kinetic energy of the ionic fragments produced by electrons with energies between 22 and 800 eV. This finding constitutes a step forward to understand the influence of shake-up and vertical transition routes to fragmentation, going beyond procedures based on adjustments of the shape of the experimental cross sections.

If a similar analysis is made for the proton case, it is observed that the ratios CH_2^+/CH_4^+, CH^+/CH_4^+, and C^+/CH_4^+ are smaller than those obtained by electron impact at the same velocity, with the C^+/CH_4^+ ratio observed to be ~ 4.5 times lower at ~ 5.5 a.u. impact velocity. This discrepancy gradually decreases as the impact velocity increases. This significant difference between projectiles with opposite charges in a dynamic regime dominated by satellite states is not at all surprising. Indeed, the dynamic role of shake-up and shake-off processes has received great attention since the 1980s due to their role in explaining the observed differences between positive and negative projectile ions in the double ionization and the ionization excitation of He and H_2 in the intermediate-velocity region [32–39]. However, this is still an inconclusive conceptual issue for two-electron systems and a fully open one for systems with many correlated electrons [39]. The most widely used explanation for those differences is based on the perturbative expansion that includes a Z^3-proportional term in the ionization cross section originating from the interference between shakeup and the ionization-excitation process usually called two-step-two (TS2), which occurs when the projectile collides with two electrons from the target, ionizing one and exciting (or ionizing) the other [32].

Signatures of shake-up processes should appear more clearly in experiments that select the products of fragmentation from the removal of a single electron (single ionization). On the other hand, shake-off processes, should appear more clearly in measurements that select the products of fragmentation due to the removal of two electrons (double ionization). Experiments that select the number of electrons removed from the target have been termed exclusive [40]. Most of the data reported in the literature do not use this discrimination. To the authors' knowledge, only the measurements of Ward *et al.* [24] for electron impact, with velocities in the 1.7-a.u. < v < 3.8-a.u range, and of Ben-Itzhak *et al.* [26] for protons, with velocities in the 6.3-a.u < v < 21.9-a.u. range, are exclusive regarding methane fragmentation. Possible contributions of interference in the fragmentation yields should be expected in a region of velocities where both processes, shake-up and

TS2, contribute significantly. The data of Ward *et al.* [24] do not reach the region of higher velocities where the shakeup dominates, whereas the velocities measured by Ben-Itzhak *et al.* [26] are not sufficiently low to indicate the presence of the TS2 process. The same applies to the case of double ionization, in this case involving the shake-off and TS2 processes.

In this work we report exclusive cross sections for all methane fragmentation channels by protons with velocities between 2.5 and 10.4 a.u., filling the gap mentioned above for the region of velocities where the effects of the charge sign on the production of the fragments are expected to be more prominent. In addition, the DETOF (delayed extraction time-of-flight) technique [41–43] allowed us to open a path in this type of investigation by obtaining distinct signatures of the vertical and satellite transitions in the kinetic energy distribution of the ionized fragments produced by electron impact.

II. EXPERIMENT

A. Electron impact

The electron collisions experimental setup has been described thoroughly before [41–44] and only a brief description is included here. It is composed by a standard time of flight (TOF) mass spectrometer, coupled to a pulsed electron gun operating in the 22–800 eV energy range, and a gas cell at room temperature. An upgrade on the experimental setup [44] allowed more precise measurements, including an extended impact energy range, than previously taken data [9].

The positively charged ions produced during the collision are guided through the TOF drift tube by a pulsed electric field of approximately 50 kV/m and a rising time of 100 ns, and are detected by a microchannel plate (MCP) detector. The whole spectrometer efficiency, comprising the detector's efficiency and the losses on the apparatus, was obtained, for the different mass-to-charge ratios, via a procedure described in a previous work [44]. To ensure that all measurements were taken in a single-collision regime, the gas cell pressure was kept below $\sim 2 \times 10^{-4}$ Torr, while the electron beam produced 50-ns pulses with a repetition rate of 2×10^4 Hz. The electrons were collected by a Faraday cup, and the pressure inside the gas cell was measured by an absolute capacitive manometer, and therefore ionization and fragmentation absolute cross sections could be directly obtained.

The kinetic energy distributions (KED) of the produced fragments in the collision processes could be measured employing the DETOF technique [41,42]. The DETOF procedure consists of systematically and gradually increasing the delay time between the electron-beam pulse and the extraction field pulse. This allows fragments with higher velocities enough free-flight time to leave the interaction region before the extraction field is turned on—thus, this time delay can be employed as a velocity selector and the different velocity distributions that compose the total fragment yield can be found. Since the number of detected ions, in this procedure, depends on the integral of the original velocity distribution of the produced fragment, trial functions have to be used and analyzed numerically [41–43]. Three types of energy

TABLE I. Absolute cross sections (in Mb) for CH$_4$ ionization and fragmentation by electron impact for the different electron impact energies, E, with the combined results of previous [9] and present measurements. Whenever present and previous results diverge, those presented here should be used. Uncertainties are found to be 7% for CH$_2^+$, CH$_3^+$, and CH$_4^+$, and 9% for C$^+$ and CH$^+$.

E (eV)	C$^+$	CH$^+$	CH$_2^+$	CH$_3^+$	CH$_4^+$
22	–	–	3.31	57.1	93.1
26	–	2.10	7.90	92.6	129
30	0.53	3.24	13.5	111	145
35	1.37	7.30	22.0	119	150
40	2.74	12.0	26.9	128	161
50	4.20	15.4	30.5	133	164
60	5.18	17.2	33.2	138	168
70	5.68	18.0	34.2	138	169
100	6.42	17.9	32.7	137	166
150	5.65	15.0	28.5	121	149
200	4.63	12.1	24.5	110	138
300	3.26	8.79	20.1	92.1	111
400	2.28	6.55	15.3	78.3	95.0
500	1.82	5.19	12.4	67.0	81.4
600	1.42	4.20	11.1	61.0	72.1
800	1.00	3.21	8.53	47.7	57.1

distribution functions have been used and associated with the DETOF technique: Maxwell-Boltzmann (MB), with no free parameters and corresponding only to nonfragmented moieties, which as a consequence acquire no kinetic energy in the collision process; exponential (henceforth referred to as Expo), assigned to fragments with suprathermal kinetic energy, representing species that gain minimum kinetic energy as fragmentation occurs; and Gaussian (henceforth referred to as Gauss), accounting for more violent fragmentation processes, in which the fragments gain relevant amounts of kinetic energy due to momentum conservation and transfer.

In this particular case, the only observed species with a MB distribution is the parent molecular ion, CH$_4^+$, while all the others present either one or two of the other available energy distributions, with different parameters. All distributions were obtained keeping their R^2 adjustment [45] with respect to the experimental data above 0.99, and uncertainties were estimated by keeping $R^2 > 0.97$.

The absolute ionization and fragmentation cross sections for all observed moieties of methane fragmentation by electron impact, in the impact energy range mentioned above, can be seen in Table I. These results expand the previous data measurements [9] for higher impact energies, which are needed for the velocity projectile impact comparison with protons further on, as well as providing cross sections for more intermediate impact energy values.

The DETOF technique provided information on the different energy distributions which are present for each measured fragment. As stated above, the parent molecule, which undergoes no fragmentation, retains a MB distribution, which works as a verification check of the experimental data and the data analysis. All other fragments can be described by a combination of an exponential and a gaussian distribution,

TABLE II. Fragmentation fractions corresponding to the exponential (f_1) and Gaussian (f_2) kinetic energy distributions present for fragments CH_2^+, CH^+, and C^+ produced by electron-impact ionization of methane. Uncertainties are found to be 8% for CH_2^+ and CH^+, and 10% for C^+.

E	C^+		CH^+		CH_2^+	
(eV)	f_1	f_2	f_1	f_2	f_1	f_2
22	1.00	0.00	1.00	0.00	1.00	0.00
26	1.00	0.00	1.00	0.00	0.90	0.10
30	1.00	0.00	0.90	0.10	0.72	0.28
35	1.00	0.00	0.81	0.19	0.54	0.46
40	0.92	0.08	0.78	0.22	0.50	0.50
50	0.88	0.12	0.74	0.26	0.46	0.54
60	0.85	0.15	0.70	0.30	0.42	0.58
70	0.84	0.16	0.65	0.35	0.39	0.61
100	0.82	0.18	0.62	0.38	0.33	0.67
150	0.80	0.20	0.62	0.38	0.33	0.67
200	0.80	0.20	0.62	0.38	0.33	0.67
300	0.80	0.20	0.62	0.38	0.33	0.67
400	0.80	0.20	0.62	0.38	0.33	0.67
500	0.80	0.20	0.62	0.38	0.33	0.67
600	0.80	0.20	0.62	0.38	0.33	0.67
800	0.80	0.20	0.62	0.38	0.33	0.67

which can be written as

$$f(E) = f_1 \left[\alpha_1 e^{-\alpha_1 E} \right]$$
$$+ f_2 \left[\frac{2\alpha_2}{\sqrt{\pi}[1 + \mathrm{erf}(\alpha_2 E_G)]} e^{-\alpha_2^2(E-E_G)^2} \right], \quad (1)$$

where α_i and E_G are adjustable parameters of the data analysis. For example, the CH_3^+ fragment comprises only a single exponential energy distribution (Expo), with $\alpha_1 = 28.7$ eV^{-1} and an average kinetic energy of 0.035 eV [9]. Since there is no Gaussian distribution needed in order to describe the experimental data for CH_3^+, $f_1(CH_3^+) = 1$ and $f_2(CH_3^+) = 0$ for all impact energies. The remaining fragments—CH_2^+, CH^+, and C^+—have both distributions, exponential and Gaussian, present throughout the impact energy range observed here. These fractions are listed in Table II for each fragment. The corresponding cross sections for each fragment ion (fgm) are $\sigma_{Expo}(fgm) = f_1\sigma(fgm)$ and $\sigma_{Gauss}(fgm) = f_2\sigma(fgm)$, where $\sigma(fgm)$ is given in Table I.

The increase in the impact energy not only allows new fragmentation channels to open up, but also modifies their relative cross sections. These are reflected in the change in the relative yield of fragments with different kinetic energy distributions. The average kinetic energy for all exponential distributions for these three fragments (corresponding to the f_1 fractions displayed in Table II) are found to be $1/\alpha \approx 35$ meV, which corresponds to ≈ 11 meV in the center of a mass system, a value compatible with the 8 meV reported in Ref. [7]. The Gaussian distributions (indicated by f_2 on the same table) have an average kinetic energy of $E_G = 200$ meV for CH_2^+ and CH^+, and 250 meV for C^+, also compatible with the value of 180 meV reported by Xu *et al.* [7]. It must be noted that the average width of the Gaussian distribution for C^+ increases slightly from 70 to 150 eV impact energy,

indicating that other C^+ production channels may open up in this energy range, but the experimental apparatus does not have enough resolution to discriminate them.

The above results correspond to *singles* measurements. The transmission of H^+ ions is strongly depleted due to the minimum delay of 300 ns used, a value constrained by the decay time of the extraction field pulse. Fast H^+ ions released in double ionization escape from the extraction region within this time interval and are not recorded.

B. Proton impact

As in the case of electron impact, the experimental setup used for protons in this work has been described previously [46–48]; therefore only a brief summary will be given here. A proton beam with energies ranging from 250 up to 2500 keV and a CH_4 effusive jet are set to cross at right angles on the focus of a time-of-flight mass spectrometer. After the ionization of CH_4, the ejected electrons and ionic fragments are extracted to opposite directions by a static electric field of 70 kV/m. The electrons are focused and detected by an electron multiplier detector, while the ionic fragments are accelerated towards a field-free drift tube and further detected by a microchannel plate detector. With a multihit coincidence setup based on a fast time to digital converter (TDC), two time-of-flight spectra can be obtained, setting the emitted electron(s) as the start pulse input and the ionic fragments (recoil ions) as the sequential multihit STOP input signals (e.g., $H^+ + CH_3^+$), where the H^+ recoil provides the first stop and the CH_3^+ recoil provides the second stop. In the first case, a *singles* spectrum is produced from events in which only a single ion arrived at the detector following ionization. In the second case, two ions arrive at the detector following double or triple ionization, generating ion-*pair* coincidence spectra. The ion-pair spectra are displayed as two-dimensional histograms with the time of flight of the first detected ion T1 plotted on the *y* axis, and the time of flight of the second detected ion T2 plotted on the *x* axis.

Nevertheless, it is important to take into account the fact that the detection efficiencies of the recoils ions and electrons are not 100%. This can lead to a scenario where the lack of a sequential detection of one ion of a pair might contribute as a false event to the *singles* spectrum, e.g., when H^+ or CH_3^+ are not detected. Thus, a double charge event ($q = +2$) will be measured as a single charge event ($q = +1$), producing an artificial enhancement of single-ionization channels, such as $CH_4^+ \rightarrow H^+ + CH_3$ or $H + CH_3^+$. As a consequence, it is necessary to correct the measured ion yields to the detection efficiencies, in order to obtain the true ion yields.

The procedure to correct the measured yields relies on obtaining the detection efficiencies for the recoil ion ϵ_1 and for the electron ϵ_2. The detection efficiencies account for the transmission efficiency of the grids, as well as the efficiency of the detector(s) and electronics. The values of ϵ_1 and ϵ_2 were determined by carrying out separate measurements.

For the recoil ion case, we used the data of Ref. [26] to obtain the detection efficiency. We noted that although the MCP is set to work at the saturation mode [46], the efficiencies for detection of CH_n^+ and the H^+ recoils are different. The value of ϵ_1 was assumed to be ϵ_H and ϵ_{ion}

for H$^+$ and CH$_n^+$, respectively. These efficiencies were obtained by normalizing the sum of ion-pair production ratios Σ_n [S(H$^+$ + CH$_n^+$)/S(CH$_4^+$)] and the ratio of single H$^+$ production, S(H$^+$)/S(CH$_4^+$), to the data of Ref. [26], taking the energy of 2.5 MeV as reference. S denotes the area under the peak in the time-of-flight spectra. The values of ϵ_H and ϵ_{ion} varied from 0.17 to 0.13 and from 0.26 to 0.20, respectively, during the data acquisition.

The electron detection efficiency ϵ_2 was obtained by comparing the yield of single ionization of neon (Ne$^+$) by proton impact, using two different START-STOP signal arrangements measured simultaneously: one arrangement with e as START and Ne$^+$ as STOP, the other with proton as START and Ne$^+$ as STOP. As the proton signal was obtained using a solid-state detector, an efficiency of 100% was assured as long as the counting rate was kept below 2000 particles per second. Therefore the ratio between these yields provides the value for ϵ_2 as ϵ_1 cancels out. The values obtained along the measurements varied from 0.2 to 0.3.

Using the channels CH$_4^+$ $\rightarrow$ H + CH$_3^+$ as an example for the single-ion production and CH$_4^+$ $\rightarrow$ H$^+$ + CH$_3^+$ for the ion-pair production, the true areas can be written in terms of ϵ_1 and ϵ_2 as follows:

$$S^{true}(\text{CH}_3^+) = \frac{S^{meas}(\text{CH}_3^+)}{\epsilon_2 \epsilon_{ion}}$$
$$- \left(\frac{\left[\epsilon_2^2 + 2\epsilon_2(1-\epsilon_2) \right] [\epsilon_{ion}(1-\epsilon_H)]}{\epsilon_2 \epsilon_{ion}} \right)$$
$$\times S^{true}(\text{H}^+ + \text{CH}_3^+),$$

where S^{true} is the true area for single-ion CH$_3^+$ + H production. The probability of detecting only a single ion, CH$_3^+$, from the H$^+$ + CH$_3^+$ ion pair is given by $\epsilon_{ion}(1-\epsilon_H)$ (detecting CH$_3^+$ AND not detecting H$^+$) multiplied by $\epsilon_2^2 + 2\epsilon_2(1-\epsilon_2)$, which accounts for the detection of either two or one of the two emitted electrons.

The true areas for H$^+$ + CH$_3^+$ ion-pair production is given by

$$S^{true}(\text{H}^+ + \text{CH}_3^+) = \frac{S^{meas}(\text{H}^+ + \text{CH}_3^+)}{\epsilon_H \epsilon_{ion} \left[\epsilon_2^2 + 2\epsilon_2(1-\epsilon_2) \right]}. \quad (2)$$

In Eq. (2), the $\epsilon_2^2 + 2\epsilon_2(1-\epsilon_2)$ term also accounts for the detection of either two or one of the two emitted electrons, and $\epsilon_H \epsilon_{ion}$ accounts for the sequential detection of the H$^+$ and CH$_3^+$ ion pair. Similar sets of equations can be written for all single-ion and ion-pair yields.

The cross sections were obtained by normalizing the true yields to the total-ionization cross section of Rudd *et al.* [49] for each energy measured in this work. The cross sections for single and double ionization are listed in Tables III and IV, respectively.

III. RESULTS AND DISCUSSION

A. Total ion production

Our present measurements for the total (nonexclusive) CH$_3^+$, CH$_2^+$, CH$^+$, and C$^+$ ratios, with respect to the parent

TABLE III. Absolute cross sections (in Mb) for CH$_4$ single ionization and fragmentation by proton impact for the different proton impact energies [E (keV)]. Uncertainties are found to be 15% for CH$_2^+$, CH$_3^+$, and CH$_4^+$, and 20% for C$^+$ and H$^+$.

E (keV)	H$^+$	C$^+$	CH$^+$	CH$_2^+$	CH$_3^+$	CH$_4^+$
150	39	3.4	16	40	217	275
250	33	2.6	11	33	178	209
350	18	1.1	6.1	19	115	140
426	19	1.1	7.9	22	139	170
500	15	1.0	5.5	19	116	140
750	11	0.59	4.0	14	93	112
1000	7.1	0.39	2.8	9.9	71	86
1500	4.7	0.36	2.1	7.6	52	63
2500	3.4	0.28	1.4	5.0	35	42
2700	5.5	0.22	1.3	4.4	32	37

ion CH$_4^+$, as a function of the projectile velocity are show in Fig. 1. This figure also includes these ratios taken from previous measurements by several authors for both electron [10,22–24] and proton [25–28] impact. In order not to overload the figure, some earlier measurements which presented significant discrepancies with the most recent ones are not shown.

Several dynamic features behind the production of these fragments are revealed in this figure. First, an overview of similarities and differences between the two projectiles can be made by separating the displayed range of velocities in three regions. At low velocities, the ratio for proton impact dominates for all fragment ions because of their lower threshold velocity due to their higher mass compared to electrons. For intermediate velocities, 2 a.u. $< v <$ 10 a.u., differences between electrons and protons are imperceptible for CH$_3^+$ and slightly above the experimental uncertainties for CH$_2^+$. CH$^+$ and C$^+$, on the other hand, are clearly more abundantly produced by electrons compared to protons, this difference being more pronounced for C$^+$. For higher velocities, and for all fragment-ion ratios, the measurements indicate a tendency of coalescence for the two projectiles, as shown by the data of Refs. [22,26].

TABLE IV. Absolute cross sections (in Mb) for CH$_4$ double ionization and fragmentation by proton impact for the different proton impact energies E. Uncertainties are found to be 20%, except for CH$^+$ + H$_2^+$, which is 45%.

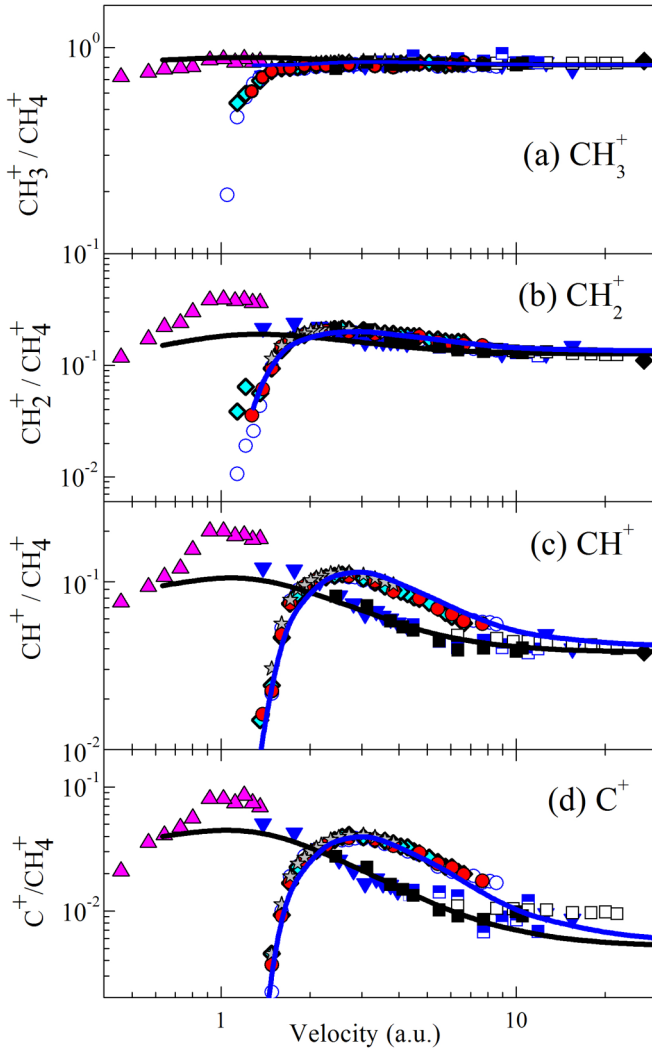| E (keV)	CH$_3^+$ +H$^+$	CH$_2^+$ +H$^+$	CH$^+$ +H$^+$	C$^+$ +H$^+$	CH$_2^+$ +H$_2^+$	CH$^+$ +H$_2^+$
150	14	17	7.1	4.1	2.2	2.1×10^{-01}
250	7.8	8.9	4.0	2.1	1.6	1.3×10^{-01}
350	3.8	4.9	2.0	1.2	–	–
425	3.6	4.5	1.9	1.0	0.67	–
500	3.0	3.9	1.7	0.87	0.68	7.3×10^{-02}
750	1.6	2.1	0.93	0.55	0.38	3.6×10^{-02}
1000	0.95	1.2	0.61	0.34	0.22	1.8×10^{-02}
1500	0.51	0.64	0.30	0.16	0.090	1.4×10^{-02}
2500	0.33	0.42	0.24	0.14	0.078	6.8×10^{-03}
2700	0.24	0.31	0.19	0.12	0.065	3.8×10^{-03}

FIG. 1. Ratios between fragment-ion-production cross sections and the parent-ion CH_4^+ cross section as a function of the projectile velocity. Experiment for proton impact: black closed squares, this work; open squares, Ref. [26]; half-filled blue squares, Ref. [28]; magenta closed up triangles, Ref. [25]; blue closed down triangles, Ref. [27]. Experiment for electron impact: red closed circles, this work; stars, Ref. [24]; cyan closed diamonds, Ref. [23]; open circles, Ref. [22]; open diamonds, Ref. [10]. Solid curves are total cross-section ratios from this work as discussed in Sec. III D: black, protons; blue, electrons.

Second, the association between the production of each fragment and the molecular orbital where the primary vacancy was produced can be roughly identified. Our data, together with those of Tian and Vidal [23] and Straub et al. [22], indicate that the threshold for the production of fragments, by electron impact, occurs for $v \sim 1$ a.u. in the cases of CH_3^+ and CH_2^+ and clearly moves towards higher velocities for CH^+ and C^+. $v \sim 1$ a.u. corresponds to the vertical transition $(1t_2)^{-1}$, which has a binding energy of $E_b = 12.62$ eV [15]. This orbital, therefore, has a negligible participation for the production of CH^+ and C^+, which are dominated by energy transfers close to the ionization of the orbital $2a_1$, as already pointed out long ago [10].

Finally, the role of single or double ionization in the production of the fragments can also be visualized. As shown in Ref. [50], the shape of the cross-section ratios versus the projectile energy is an indicator of the dominant mechanism for the production of a particular fragment ion. Figure 1 shows that, for CH^+ and C^+, there is a clear change in the concavity of the ratios towards a high-velocity regime for both electrons and protons. For higher velocities, the ratios are constant, indicating that the production of the fragment ion occurs via single ionization, having the same velocity dependence of the parent-ion production.

Single ionization induces either vertical transitions from a given molecular orbital or one-electron–two-vacancy shake-up states. It should be noted that the ratios included in this figure do not discriminate whether a fragment ion resulted from the molecular breakup of a single or doubly ionized intermediate state. In the latter case, the production of fragment ions by swift projectiles would be dominated by populating shake-off states or by a postcollisional process such as Auger decay.

For velocities below where the concavity changes, the ratios increase as the velocity decreases, exhibiting $\sim v^{-2}$ dependence for both projectiles. This stronger dependence on velocity than that associated with single ionization indicates the predominance of a double collision, a two-step process where the projectile interacts twice. This process has been called TS2 [32] and will be designated herein for double ionization and ionization excitation as well. The displacement at high velocities of the inflection point observed in C^+ when compared to CH^+ is due to the different relative contributions of TS2 and single ionization in the production of each of these fragments. Again, there is no discrimination in these plots between the double-ionization or ionization-excitation contributions to TS2. In order to better study these processes, it is necessary to separate the fragment fractions originating from double ionization from those from simple ionization. This is the object of the following sections.

B. Double ionization

The present exclusive measurements for proton impact are shown in Figs. 2 and 3, together with those of Ben-Itzhak et al. [26] and those of Ward et al. [24] for electron impact. These figures show the ratios between the $CH_n^+ + H^+$ and $CH_n^+ + H_2^+$ double-ionization cross sections and the total-ionization cross section. Panel (h) of Fig. 3 displays the ratio between total double-ionization and total-ionization cross sections (R_{DT}).

The observation of Figs. 2 and 3 clearly show two well-identified dynamic regions. For $v \gtrsim 8$ the data from Ref. [26] are constant, indicating a postcollisional double ionization that will be assigned here to the Auger decay of the carbon K shell. For $v \lesssim 8$, our data show that the ratio has a dependence on the velocity of the projectile in the form $\sim v^{-2}$, which will be assigned here to the TS2 mechanism. Next, these two regions are closely analyzed with the purpose of obtaining the branching ratios for each one of the cationic moieties measured.

The ionization cross section of the carbon K shell by protons, σ_K, can be obtained with the aid of the first Born
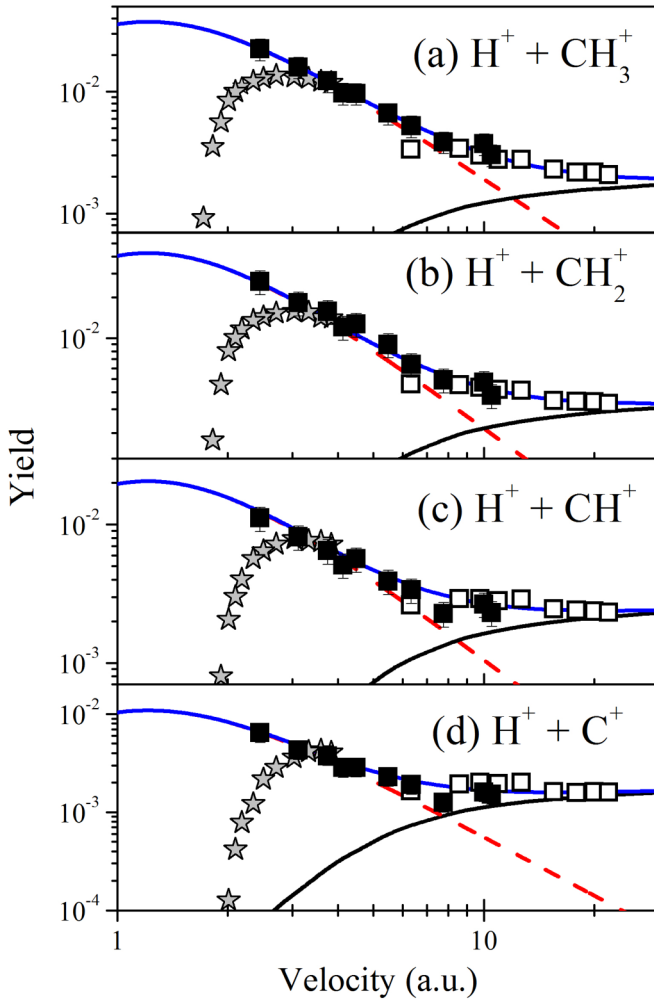
FIG. 2. Ratios between double-ionization cross sections corresponding to various fragmentation channels and the total-ionization cross section as a function of the projectile velocity (yields). Experiment: closed squares, this work for proton impact; open squares, Ref. [26] for proton impact; stars, Ref. [24] for electron impact. Theory for proton impact: solid black curves, K-shell contributions (see text); dashed red curves, TS2 contributions (see text); solid blue curve: total calculated yields.

approximation along with the binding energy correction as proposed in Ref. [51]. These calculations, added to the fluorescence yield given by Krause [52], are in excellent agreement with the measurements of the carbon K-shell x-ray production cross sections reported by Yu *et al.* [53]. In the following it is assumed that all single vacancies produced in the K shell relax via Auger decay in CH$_4{}^{2+}$, which subsequently fragments into two charged and a number of neutral species, according to some yield that is found next and denoted by f_A.

The K-shell ratios shown in Figs. 2 and 3 can be calculated using the scaling suggested in Ref. [54] to estimate the total-ionization cross section by protons, σ_I:

$$\frac{\sigma_{MO}I^2}{Z_{MO}\delta_{MO}} = \frac{A\ln(1+Bx)}{x} - \frac{AB}{(1+Cx)^4}, \qquad (3)$$

with $A = 11\,500$, $B = 0.09$, $C = 0.012$, $x \times (E/M)/I$, E/M in keV/amu, and ionization energies of $I = 12.616/13.6$ Ry
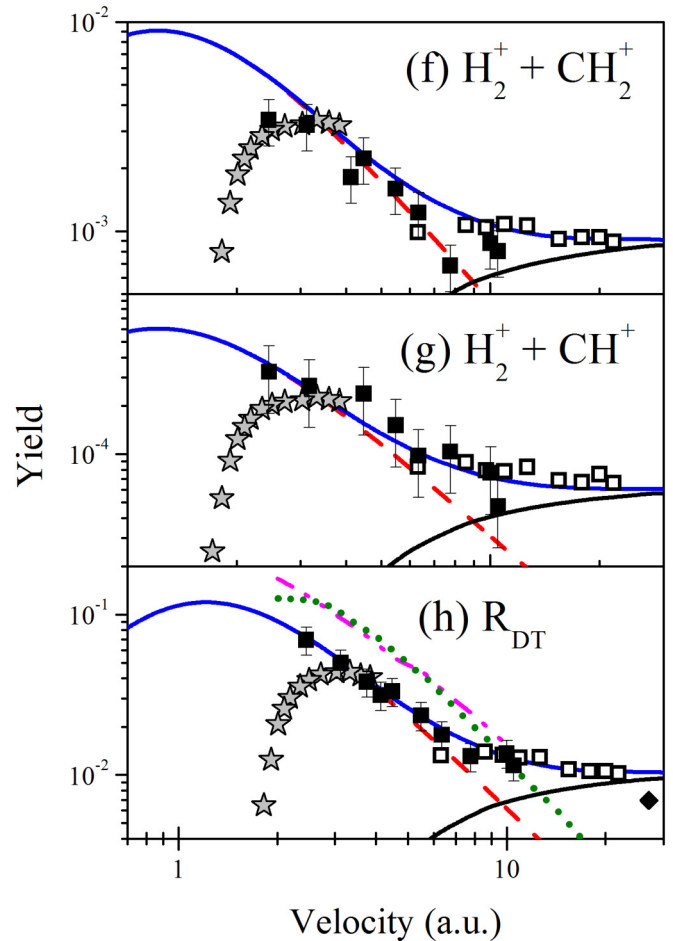
FIG. 3. (f, g) Same as Fig. 2. (h) Ratio R_{DT} between double- and total-ionization cross sections. Symbols are the same as Fig. 2, with the open star from Ref. [10], for electron impact. Dashed double-dot pink curve shows calculations from Ref. [31] and dotted green curve shows calculations from Ref. [29].

for $1t_2$ and $I = 22.39/13.6$ Ry for $2a_1$ orbitals [15], giving σ_{MO} in Mb. The label MO represents a particular molecular orbital. Z_{MO} is the number of electrons in each molecular orbital, 6 for $1t_2$ and 2 for for $2a_1$, and δ_{MO} is an adjustment parameter taken as 0.5 in all cases. With these parameters an excellent agreement is obtained with the total-ionization cross sections (σ_I) reported by Luna *et al.* [28] and Rudd *et al.* [49]. The K-shell Auger yields for each produced ion pair is obtained by adjusting the ratios $f_A\sigma_K/\sigma_I$ to the high-energy data of Ref. [26]. The resulting f_A are given in Table V, and the adjusted curves are shown as dotted lines in Fig. 2.

The contribution from the direct TS2 mechanism is estimated along the same lines previously used [28,55], through the ratio R_{DS} between double- and single-ionization cross sections, but generalized to include the case of electron impact:

$$R_{DS} = \frac{D(v - v_0)^{2\alpha}}{[1 + F(v - v_0)^2]^{\alpha+1}}. \qquad (4)$$

For protons $v_0 = 0$ and Eq. (4) reduces to the same form used in Ref. [28]. The TS2 yields for each produced ion pair is obtained by adjusting the ratios $f_{DI}R_{DT}$ to our present

TABLE V. Ion-pair yields induced by double ionization of methane through Auger decay of K-shell (f_A) and TS2 (f_{DI}) mechanisms.

	This work		Ref. [28]	
	f_{DI}	f_A	f_{DI}	f_A
$CH_3^+ + H^+$	0.310	0.180	0	0
$CH_2^+ + H^+$	0.350	0.319	0.480	0.480
$CH^+ + H^+$	0.170	0.240	0.272	0.272
$C^+ + H^+$	0.009	0.165	0.128	0.128
$CH_2^+ + H_2^+$	0.075	0.090	–	–
$CH^+ + H_2^+$	0.005	0.006	–	–
Total	1	1	0.880	0.880

measurements. $R_{DT} = R_{DS}/(1 + R_{DS})$ is the double-to-total-ionization ratio. As in the f_A case, the sum of f_{DI} for all channels is constrained to be 1. The same parameters $\alpha = 1.5$, $D = 0.7$, and $F = 1.04$ are used for all channels listed in Table V. For electrons, $v_0 = 1.2$, $\alpha = 2.0$, $D = 0.08$, and $F = 0.5$. These values, with the same parameters displayed in Table V, reproduce quite well the measured yields of Ref. [24]. It is assumed that the final states induced by protons and electrons relax in the same way and thus the same branching ratios given in Table V are used for both projectiles.

The good agreement with the experimental data obtained by the composition of the TS2 mechanism with the postcollisional K-Auger decay for all the channels shows, from a quantitative level, the relative role of these two mechanisms in the production of ion pairs. In addition, the difference between the values obtained for f_A and f_{DI} for the various channels shows that the double vacancy distributions resulting from the TS2 and Auger mechanisms are different. This result represents progress from the simpler hypothesis adopted in Ref. [28], where $f_A = f_{DI}$ was assumed. The values obtained from Ref. [28] are reproduced in Table V for comparison. Panel (h) of Fig. 3 is included because it allows a more direct comparison between the measured data and theoretical calculations for the total double and total ionization cross sections. To date, very few calculations for double and single ionization cross sections of methane have been reported. The theoretical results from Salehzadeh and Kirchner [31] and from Gulyas *et al.* [29], displayed in Fig. 3(h), do not include the K-shell contribution. In the high-velocity region where TS2 dominates, both calculations show approximately the same energy dependence as our estimate for TS2, but with a tendency to overestimate R_{DT}.

It is remarkable to note that the double-ionization measurements reported by Ward *et al.* [24] for swift electron impact clearly coalesce with our data for all measured fragmentation channels. This finding clearly indicates that the significant differences observed and previously noted between the impact of electrons and protons are not related to double ionization. Single ionization is studied next to further clarify the effect of the sign of the projectile charge on fragmentation.

C. Single ionization

As in the case of double ionization, exclusive measurements of methane single-ionization cross sections are quite
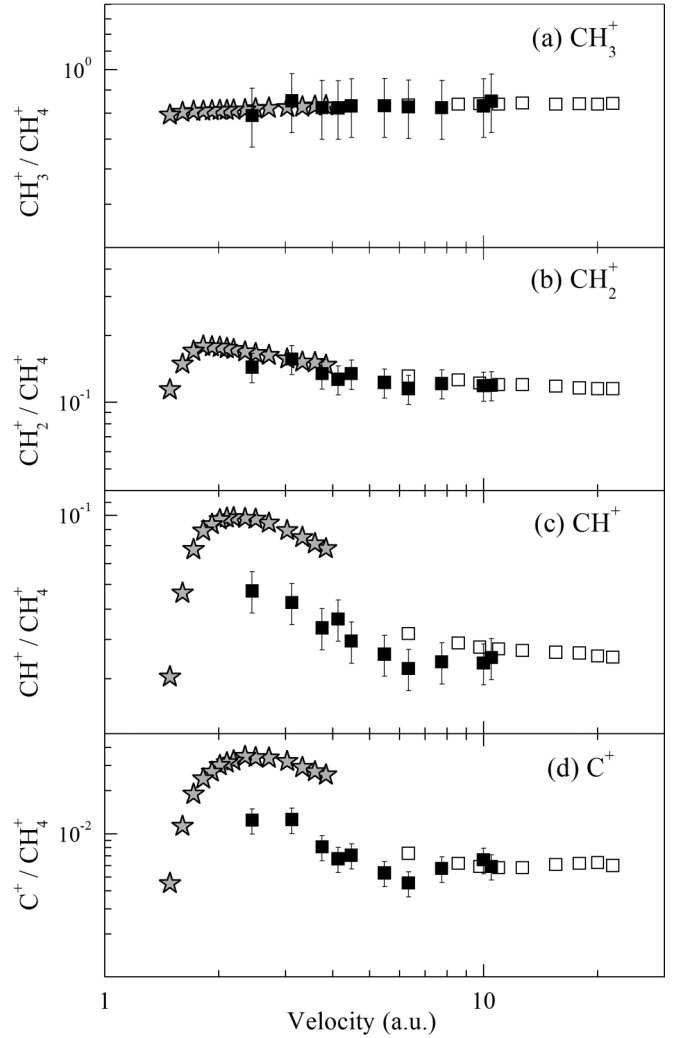

FIG. 4. Ratios between single-ionization cross sections corresponding to various fragmentation channels and the parent-ion CH_4^+ cross section as a function of the projectile velocity. Experiment: closed squares, this work for proton impact; open squares, Ref. [26] for proton impact; stars, Ref. [24] for electron impact. While differences between electron and proton impact are not relevant in panels (a) and (b), they are clear in panels (c) and (d).

scarce. Figure 4 shows our present measurements, along with those of Ben-Itzhak *et al.* [26] for protons and those of Ward *et al.* [24] for electrons, for the ratios between the cross section for the single fragment-ion production and the cross section for CH_4^+ production as a function of the projectile velocity.

Unlike double ionization, the single-ionization ratios do not show the same behavior for all fragmentation channels. In the case of CH_3^+ the ratio is essentially constant, supporting the previous assumption [10,28] that both CH_3^+ and CH_4^+ are produced solely by the ionization of the $1t_2$ orbital. It should be noted that there is no difference, within the experimental uncertainties, in the impact of electrons or protons.

This scenario changes progressively and drastically as the number of carbon-bound hydrogens decreases. First, the ratios for electron impact become progressively larger than those for proton impact at intermediate velocities, reaching a factor of ~ 2 for C^+ at $v \sim 3$ a.u. Second, our data show that a
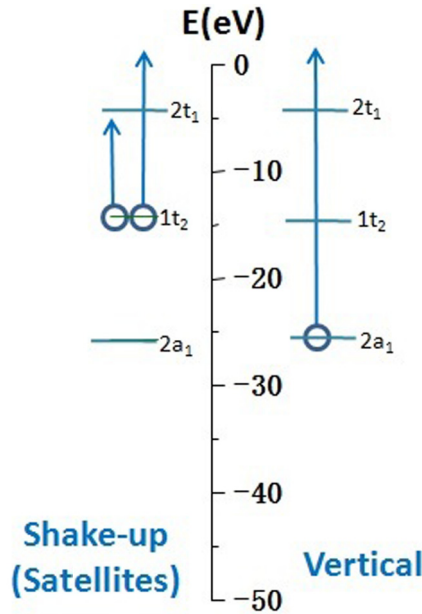
FIG. 5. Pictorial illustration of methane fragmentation via vertical transition $(2a_1)^{-1}$ or satellite states, $(1t_2)^{-2}(2t_1)$, for example. In analogy with the case of water [18], there may be a strong angular rearrangement before the ejection of the fragments in the case where the satellite states are the populated ones.

point of inflection appears for $v \sim 8$ a.u., resembling the behavior found in double ionization. This points towards the contribution of a TS2 mechanism, in this case excitation ionization. For $v \gtrsim 8$ a.u., the data of Ref. [26] show that all ratios become constant, indicating that the fragment-ion production occurs through single ionization.

These findings can be addressed conceptually through the perturbative expansion of the collision process, as previously studied for systems with fewer electrons [32–38]. It will be assumed that the fragmentation may be either due to a vertical transition, from the orbital $2a_1$, or from satellite states, energetically close to the state $(2a_1)^{-1}$, and populated via a shake-up process. These two possibilities are illustrated in Fig. 5. Satellite one-electron–two-vacancy states can also be populated by a TS2-type mechanism when the projectile interacts consecutively with two electrons, ejecting one of them and exciting the other. This mechanism is indistinguishable from the shake-up mechanism and gives rise to an interference term proportional to Z_p^3, where Z_p is the projectile charge. The interference term is positive for electrons and negative for protons [32,33].

Within this approach, the cross section σ_{SI} for single ionization can be written as

$$\sigma_{SI} = \sigma_{\text{vert}} + \sigma_{su} + \sigma_{ei} \pm \sigma_{\text{int}}, \quad (5)$$

where σ_{vert}, σ_{su}, σ_{ei}, and σ_{int} are the cross sections corresponding to vertical, shake-up, excitation-ionization (TS2), and interference contributions, respectively. It should be noted that these cross sections are the same for electrons and protons only in the high-velocity region. For convenience, the last two terms associated to TS2 in the above equation will be put together as $\sigma_{ei} + \sigma_{\text{int}} = \sigma_2^e$ for electrons or $\sigma_{ei} - \sigma_{\text{int}} = \sigma_2^p$ for

proton impact. σ_2^e and σ_2^p coalesce only in the high-velocity limit. In the intermediate-to-low-velocity region $\sigma_2^e > \sigma_2^p$, as suggested by this model and established by the experiment.

The corroboration of this model depends on the experimental identification of TS2 and shake-up signatures. The presence of TS2 in the production of a particular fragment is generally identified by the existence of an inflection point, at intermediate velocities, in the ratio between the fragment-ion-production cross section and the parent-ion-production cross section, as already discussed.

The experimental signature of the shakeup, on the other hand, is far more elusive. Previous studies on the production of CH$_2^+$ from methane ionization [9] and of O$^+$ from ionization of water [18] by electron impact show that competitive mechanisms behind fragmentation can be disentangled through signatures in the kinetic energy distribution of the fragment. These studies hint that vertical transitions involving inner valence orbitals are fast and impinge a measurable variation of kinetic energy in the resulting fragment ion. The fragmentation from satellite states, on the other hand, allows a geometric rearrangement of the hydrogens before fragmentation with very little increase in the kinetic energy of the fragment ions, leaving them with essentially thermal kinetic energies.

Figure 6 shows the results for ratios from exclusive single ionization, already displayed in Fig. 4, together with our results for electron impact obtained with the DETOF technique. For C$^+$, where Liu and Shemansky [17] assumed that its production came wholly from satellite states, there is remarkable agreement between the ratios obtained from the Expo distribution and those measured by Ward *et al.* [24]. This agreement suggests that the Expo distribution can be associated to fragmentation coming mainly from satellite states, populated through shakeup or TS2, including the interference contribution, i.e.,

$$\sigma_{\text{Expo}} = \sigma_{su} + \sigma_2^e, \quad (6)$$

for each fragment ion. The ratios associated to the Gauss distribution, on the other hand, correlate fairly with those for protons and will be assumed to be associated mostly with vertical transitions, i.e.,

$$\sigma_{\text{Gauss}} = \sigma_{\text{vert}}, \quad (7)$$

for each fragment ion. The destructive shake-up–TS2 interference occurring in the proton case prevents a large rise of the C$^+$/CH$_4^+$ ratio with the decrease of the projectile velocity at intermediate velocities, at variance with what happens in the electron case, where the constructive shake-up–TS2 interference significantly increases that ratio under the same kinematic conditions.

As the number of attached hydrogen increases, the relative contributions from Expo and Gauss tend to reverse. Indeed, it is the Gauss cross section that correlates quite well with the electron impact data from Ward *et al.* [24] for CH$_2^+$. Furthermore, there is no significant difference between the CH$_2^+$/CH$_4^+$ ratios for electrons and protons, meaning that TS2 and the interference terms of the ionization cross section do not contribute significantly in this case. We will consider that the assignments indicated in Eqs. (6) and (7) represent
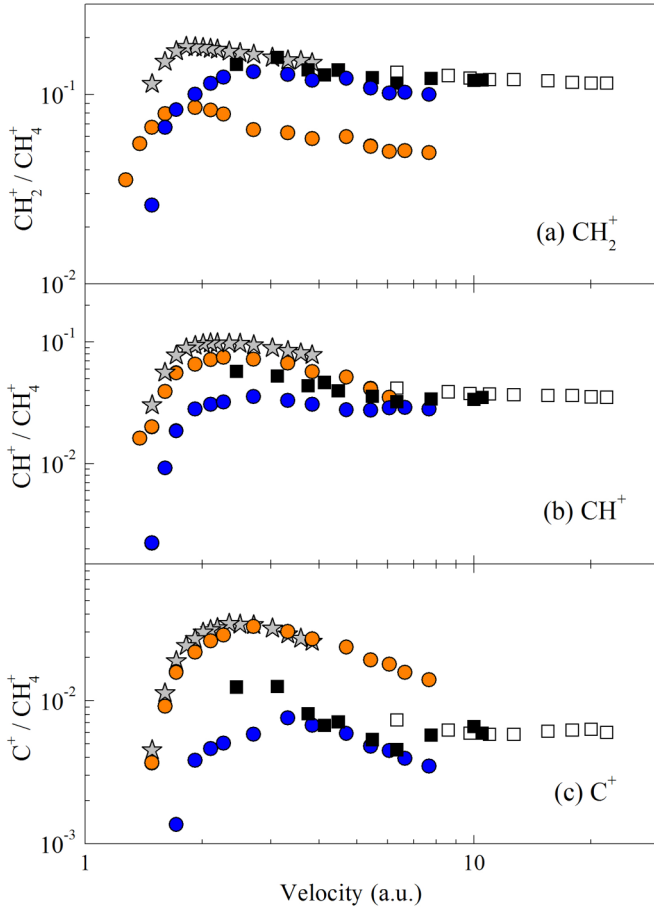
FIG. 6. Ratios between single-ionization cross sections corresponding to various fragmentation channels and the parent-ion CH_4^+ cross section as a function of the projectile velocity. Experiment: closed squares, this work for proton impact; open squares, Ref. [26] for proton impact; stars, Ref. [24] for electron impact; solid orange circles, this work for Expo contribution for the electron impact KED; blue solid circles, this work for Gauss contribution for the electron impact KED.

a good approximation for a wide range of velocities of the projectile, but that excludes lower velocities, close to the threshold. In fact, in all cases the threshold of the Expo distribution is lower than that of the Gauss. For CH_2^+ this lower threshold for the Expo is associated with the $CH_2^+ + H_2$ channel as indicated by Samson *et al.* [15], Sigaud and Montenegro [9], and Xu *et al.* [7]. In addition, a fraction of the contribution from fragmentation originating from state $(1t_2)^{-1}$ is likely to be contained in the Expo distribution.

Next, a simple model is presented to make the connection between the various contributions to single ionization and the production of ions. This model provides a closer look at this connection when compared to the decay model presented in Ref. [28].

D. A model for ion production from single ionization

The final fragment-ion-production cross section is driven by the ionization cross sections σ_{1t_2}, σ_{vert}, and σ_{su}, which coalesce for electrons and protons only at high velocities,

and by σ_2^e or σ_2^p, which are also different for the two projectiles at intermediate velocities. Each of these single-ionization mechanisms results in the production of different singly ionized states of CH_4, which subsequently relax by fragmenting into products with characteristic relative yields. If the collision time is much shorter than the relaxation time, it can be assumed that the postcollisional fragmentation is independent of the projectile charge. Thus, the fragmentation matrix corresponding to the fractions f_{1t_2}, f_v, f_{su}, and f_{ei} associated to each fragment ion produced by single ionization is the same for both electrons and protons. The fragment-ion-(fgm) production cross sections, $\sigma_{SIp}(fgm)$, can be written for the proton case as

$$\sigma_{SIp}(fgm) = f_{1t_2}\sigma_{1t_2}^p + f_v\sigma_{\text{vert}}^p + f_{su}\sigma_{su}^p + f_{ei}\sigma_2^p, \quad (8)$$

and similarly for the electron case as

$$\sigma_{SIe}(fgm) = f_{1t_2}\sigma_{1t_2}^e + f_v\sigma_{\text{vert}}^e + f_{su}\sigma_{su}^e + f_{ei}\sigma_2^e. \quad (9)$$

The cross sections $\sigma_{1t_2}^{p,e}$, $\sigma_{\text{vert}}^{p,e}$, and $\sigma_{su}^{p,e}$ can be estimated with the aid of Eq. (3). Assuming that the TS2 contributions to populate satellite states are due to the $1t_2$ orbital, $\sigma_2^{p,e}$ can be estimated by

$$\sigma_2^{p,e} = R_{DS}^{p,e}\,\sigma_{1t_2}^{p,e}, \quad (10)$$

where $R_{DS}^{p,e}$ is given by Eq. (4), with $v_0 = 0$ or $v_0 = \sqrt{I}$ for the proton or electron case, respectively. The parameters to calculate these cross sections, as well as the fragmentation matrix, are obtained by adjusting the single-ionization cross sections for each fragment ion with the present and Ref. [26] measurements for proton impact and with the present σ_{Expo} and σ_{Gauss} cross sections for electron impact. The set of parameters for the cross sections is displayed in Table VI and the fragmentation matrix in Table VII.

It should be emphasized that this simplified semiempirical model is not intended to give an accurate description of the fragment-ion cross sections but to show a consistent, comprehensive, and reasonably quantitative picture of the various mechanisms behind fragmentation. Figure 7 compares the present calculations with the measured σ_{Expo} and σ_{Gauss} contributions for CH_2^+, CH^+, and C^+ production. The results based on Eqs. (6) and (7) show that, through the adopted procedure, it is possible to quantitatively identify and separate the contributions coming from the vertical transitions from those coming from the shakeup, properly disentangled by the DETOF technique. The shake-up mechanism clearly predominates as a larger number of hydrogens are ejected, in qualitative agreement with the results of Ref. [17]. However, this reference assigns 100% of the C^+ produced to the shake-up mechanism, while our measurements indicate that some contribution due to the vertical transitions still lasts for the production of this ion. As mentioned before, full molecular fragmentation induced by *single* ionization of water [18] is also dominated by satellite states with energies close to those corresponding to a vacancy in an inner valence orbital. It seems that these satellite states are very effective in causing multiple hydrogen ejections.

Because each particular fragment is highly selective with respect to the initial state of the singly charged parent ion, an evaluation of the relative contributions from the vertical,

TABLE VI. Parameters for cross-section calculations, according to Eq. (3), corresponding to σ_{1t_2}, σ_{vert}, σ_{su}, σ_2^p, and σ_2^e.

	Protons				Electrons			
	$1t_2$	vert	su	2	$1t_2$	vert	su	2
A	13000	3900	1400	–	13000	3900	1400	–
B	0.07	0.07	0.07	–	0.038	0.07	0.07	–
C	0.0093	0.0093	0.0093	–	0.0051	0.0093	0.0093	–
I (Ry)	0.928	1.646	1.912	1.912	0.928	1.646	1.912	1.912
D	–	–	–	0.08	–	–	–	0.08
F	–	–	–	0.5	–	–	–	0.3
α	–	–	–	0.2	–	–	–	0.6

shake-up, and TS2 transitions plus interference to this initial state may be best viewed considering the sum of the production of CH$_2^+$, CH$^+$, and C$^+$, which constitutes more than 80% of the products from these processes. Figure 8 shows the ratios between the sum of the single cross sections for the production of these fragments and the CH$_4^+$ cross section, chosen as a reference for a vertical transition, $(1t_2)^{-1}$, for both electrons and protons. The empirical ratios reported by Liu and Shemansky [17] are displayed in panel (a) as dashed lines for comparison and show a very similar picture, both in shape and in absolute values, for σ_{vert} and $\sigma_{su} + \sigma_2^e$, where this last contribution was labeled as satellite in their paper. The calculated ratios for σ_{vert} and σ_{su} are rather similar for electrons and protons, with the differences at low velocities due to the much smaller threshold velocity in the latter case. The TS2 plus interference ratios, for σ_2^e and for σ_2^p, on the other hand, are very different, with the former competing with that for σ_{vert} at $v \sim 3.0$ a.u. Calculations of single-ionization cross sections usually consider only vertical transitions, neglecting the higher-order TS2 and interference terms. This may be a reasonable approximation for positively charged particles but not for negatively charged ones. Previous measurements reported by Knudsen *et al.* [27] with antiprotons also point toward this conclusion.

As mentioned in the Introduction, some previous studies on methane ionization by protons [29,31] have used the sequential decay model described by Luna *et al.* [28] which directly relates the various fragment-ion cross sections to the cross section for single ionization. A comparison between this procedure with the one described in this work is shown in Fig. 9. The fragment-ion cross sections using

the method of Ref. [28] are calculated using Eq. (3), with the parameters indicated immediately after this equation and with the branching ratios given in the Table VII, while those developed in this work, using Eq. (8), are calculated with the parameters and branching ratios displayed in Tables VI and VII, respectively. The agreement between the two procedures is quite reasonable, except for the region of the lower-energy data of the C$^+$ fragment, where a slight increase of the cross
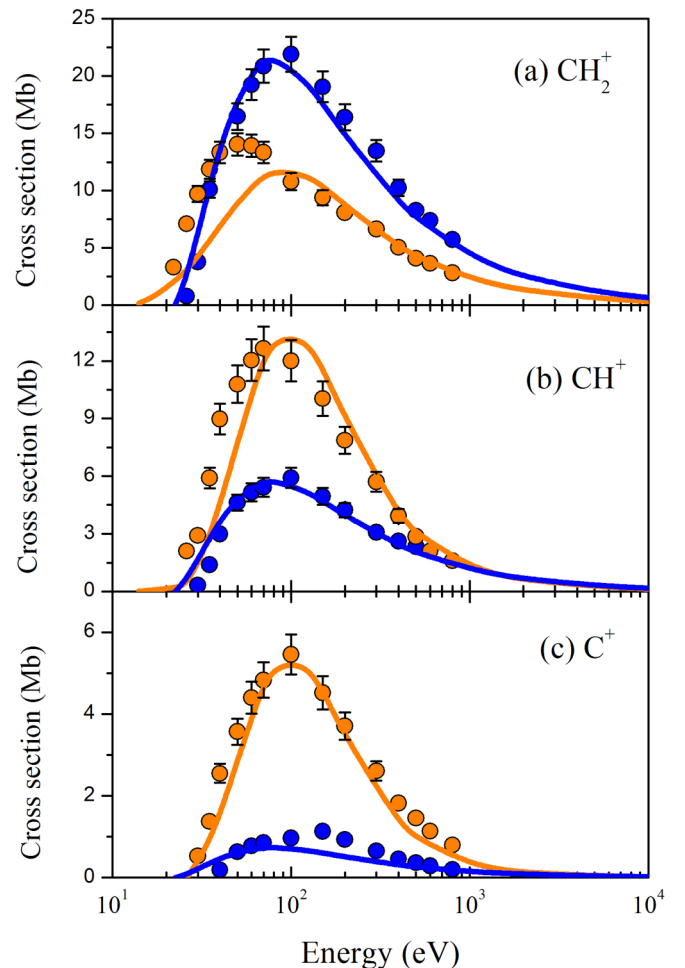

FIG. 7. Electron-impact cross sections corresponding to the two kinetic energy distributions found for each fragment ion. Experiment: σ_{Expo}, orange circles and σ_{Gauss}, blue circles. Calculations are according to Eq. (6), orange solid curves, and Eq. (7), blue solid curves.
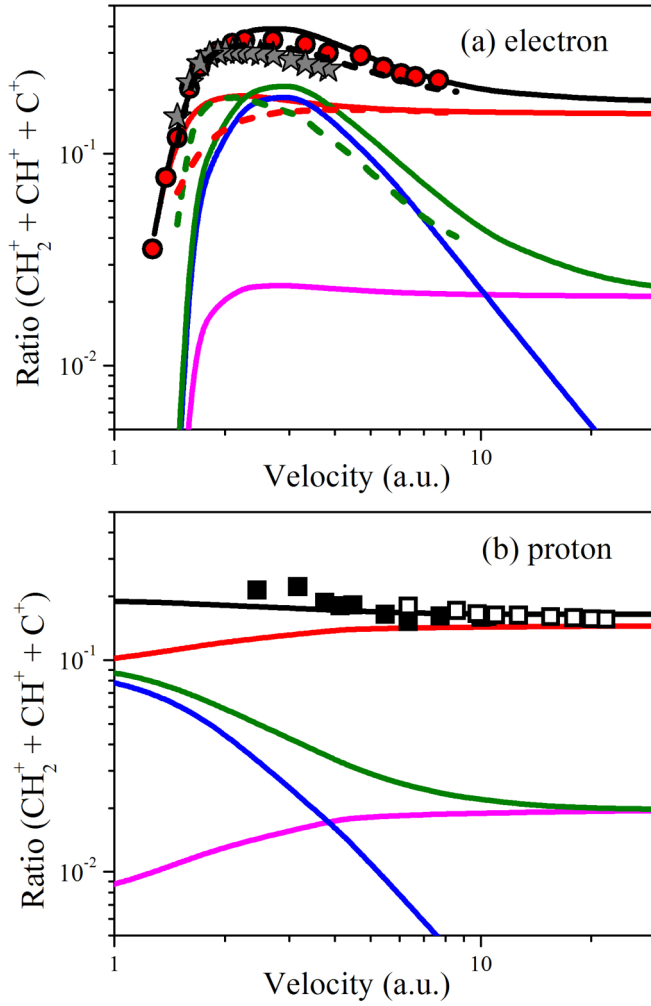
TABLE VII. Fragmentation matrix. The last columns are the branching ratios from Ref. [28] to be used with the total single-ionization cross section.

	f_{1t_2}	f_{su}	f_v	f_{ei}	Ref. [28]
CH$_4^+$	0.490	–	–	–	0.490
CH$_3^+$	0.403	–	–	–	0.4032
CH$_2^+$	0.020	0.20	0.730	0.13	0.0576
CH$^+$	0.002	0.52	0.195	0,45	0.016704
C$^+$	–	0.10	0.025	0.22	0.002496
H$_2^+$	–	0.15	0.040	0.10	
H$^+$	0.085	0.03	0.001	0.10	
Sum	1	1	1	1	0.97

FIG. 9. Proton cross sections for CH_3^+ (black), CH_2^+ (red), CH^+ (blue), and C^+ (green) production from single ionization. Solid lines: this work, Eq. (8); dashed lines, Ref. [28], Eq. (3). Experiment: solid squares, this work; open squares, Ref. [26].

FIG. 8. Cross-section ratios, $R = [\sigma(CH_2^+) + \sigma(CH^+) + \sigma(C^+)]/\sigma(CH_4^+)$, for electrons (a) and protons (b). Solid lines represent contributions from σ_{vert}, red; σ_{su}, magenta; $\sigma_2^{p,e}$, green; total, black. Dashed lines are from Ref. [17]: σ_{vert}, red; $\sigma_{su} + \sigma_2^e$, green; total, black. Experiment: electrons; this work, red circles; Ref. [24], stars; protons; black squares, this work; open squares, Ref. [26].

section, in relation to the model of Ref. [28], with the decrease of the energy of the projectile can be observed. This is mainly due to the term σ_2^p, which combines the TS2 contribution with the shake-up and the interference terms, and which were considered in greater detail here.

A comprehensive overview of the adopted procedures can be examined referring back to Fig. 1, which shows the present calculations induced by electrons and protons. The proton data from Ref. [25] are well above our curves due to electron capture, which is not included in the present model. Further, it should be pointed out that the parameters used in Table VI do not take into account differences in the appearance energies for fragments coming from the $1t_2$ orbital and are not expected to be correct for electron energies near the threshold, especially in the case of CH_3^+ production. The calculated curves are the sum of contributions that have been disentangled and contribute to provide the main dynamic characteristics indicated by the experimental data: (i) the coalescence between electrons and protons at high velocities; (ii) the change
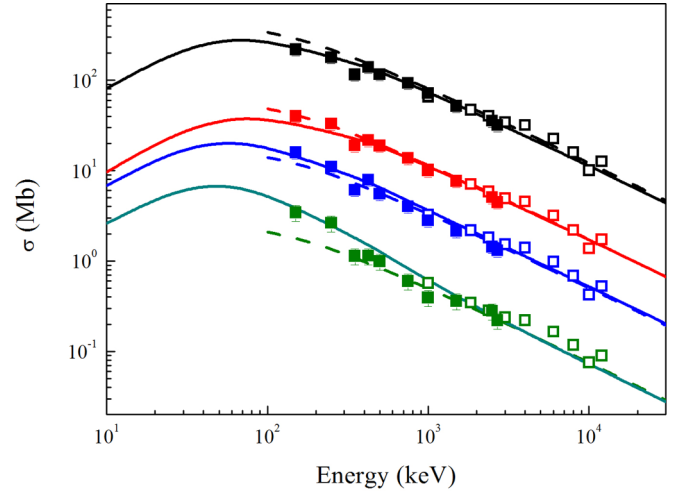
of concavity of the ratios for CH^+ and C^+ towards higher velocities, as an indication of the change of the predominant mechanism from TS2 to a single-collision regime, and (iii) the clear difference of the CH^+ and C^+ ratios for the two projectiles in intermediate energies, evidencing the effect of the charge-sign of the projectile in fragmentation. This general agreement indicates that the fragmentation matrix presented in Table VII gives a good starting point for the link between the production of ions and more sophisticated theoretical calculations for σ_{vert}, σ_{su}, and $\sigma_2^{e,p}$, when they become available, for both electron and proton impact.

IV. CONCLUSIONS

The exclusive measurements of proton-induced fragmentation along with the measurements of the fragment-ion kinetic energy distributions induced by electron impact reported here have revealed some important features related to the dynamics of the collision of charged particles with methane.

It was shown that the ionic fragments from double ionization have practically no dependence on the sign of the projectile charge. The significant difference, especially for the C^+ production cross section, observed between electrons and protons comes from single ionization. This charge-sign dependence was attributed here to interference between shake-up and double-impact mechanisms, with both processes populating satellite states energetically near the $(2a_1)^{-1}$ state. A similar process involving the shake-off and double knock-out seems to be inhibited. Due to the lack of a formal explanation for this finding at the moment, the general rule of thumb attributed to Åberg [32] can be invoked. Åberg suggests that shake-up processes dominate over the shake-off for valence electrons, which is indeed the case for the main active electrons of methane. The opposite would apply to inner-shell electrons, the K shell in the case of methane, whose vacancies essentially relax by Auger decay as discussed previously. This fast decay could interfere with double

knockout, giving rise to the same final ionic state. However, the contribution from this mechanism to double ionization seems to be below the present experimental uncertainties to be noticed.

Another longstanding issue for which a clear experimental signature had not yet been identified concerns the contribution of satellite states to the fragmentation of methane by charged particle impact. With the help of the DETOF technique it was possible to correlate and clearly separate the ionic fragments originating from the vertical transitions from those coming from the satellite states by their signatures in the kinetic energy distribution. In fact, it is remarkable that these two precursor states of fragmentation can be kinematically separated in a fairly clean way. This finding allowed quantifying the various cross sections responsible for populating states $(2a_1)^{-1}$ and $(1t_2)^{-2}(2t_1)$, among others, namely, direct ionization, shakeup, TS2, and the contribution of the interference term, this last one considered as the main source of the significant differences in fragment-ion production by electrons and pro-

tons, especially in the case of C$^+$. The clear dependence of the projectile charge-sign for the C$^+$ production has no similarity in atomic many-electron systems. Indeed, the extensive work carried out on collisions by protons, antiprotons, and electrons on noble gases [56] shows a more ambiguous scenario, as the differences in the absolute values and trends among these projectiles, both in single- and multiple-ionization cross sections, are less conclusive. The present results may open up new perspectives for the quantitative exploration of the rich and complex collision dynamics behind single and multiple ionization of many-body atomic and molecular systems induced by charged particles.

[1] A. Ll Hughes and E. Klein, Phys. Rev. **23**, 450 (1924).

[2] J. A. Hipple, Jr. and W. Bleakney, Proceedings of the American Physical Society, Minutes of Washington Meeting, April 25-29, 1935, Abstract A87 [Phys. Rev. Bd. **47**, S 802 (1935)].

[3] L. G. Smith, Phys. Rev. **51**, 263 (1937).

[4] K. Gluch, P. Scheier, W. Schustereder, T. Tepnual, L. Feketeova, C. Mair, S. Matt-Leubner, A. Stamatovic, and T. D. Märk, Int. J. Mass Spectrom. **228**, 307 (2003).

[5] B. W. Z. Chen, X. Wang, D. Lu, S. Lin, R. Hutton, and Y. Zou, J. Phys. B: At. Mol. Opt. Phys. **46**, 215205 (2013).

[6] B. Wei, Y. Zhang, X. Wang, D. Lu, G. C. Lu, B. H. Zhang, Y. J. Tang, R. Hutton, and Y. Zou, J. Chem. Phys. **140**, 124303 (2014).

[7] S. Xu, X. Ma, X. Ren, A. Senftleben, T. Pflüger, S. Yan, P. Zhang, J. Yang, J. Ullrich, and A. Dorn, J. Chem. Phys. **138**, 134307 (2013).

[8] X. Ren, T. Pflüger, M. Weyland, W. Y. Baek, H. Rabus, J. Ullrich, and A. Dorn, J. Chem. Phys. **142**, 174313 (2015).

[9] L. Sigaud and E. C. Montenegro, J. Phys. B: At. Mol. Opt. Phys. **48**, 115207 (2015).

[10] C. Backx and M. J. Van der Wiel, J. Phys. B: At. Mol. Opt. Phys. **8**, 3020 (1975).

[11] L. S. Cederbaum, W. Domcke, J. Schirmer, W. von Niessen, G. H. F. Diercksen, and W. P. Kraemer, J. Chem. Phys. **69**, 1591 (1978).

[12] L. S. Cederbaum, W. Domcke, J. Schirmer, and W. von Niessen, Phys. Scr. **21**, 481 (1980).

[13] S. T. Hood, E. Weigold, I. E. McCarthy, and P. J. O. Teubner, Nature (London) **245**, 65 (1973).

[14] S. A. C. Clark, T. J. Reddish, C. E. Brion, E. R. Davidson, and R. F. Frey, Chem. Phys. **143**, 1 (1990).

[15] J. A. R. Samson, G. N. Haddad, T. Masuoka, P. N. Pareek, and D. A. L. Kilcoyne, J. Chem. Phys. **90**, 6925 (1989).

[16] M. C. Göthe *et al.*, J. Chem. Phys. **94**, 2536 (1991).

[17] X. Liu and D. E. Shemansky, J. Geophys. Res. **111**, A04303 (2006).

[18] Natalia Ferreira, L. Sigaud, and E. C. Montenegro, J. Phys. Chem. A **121**, 3234 (2017).

[19] B. Adamczyk, A. J. H. Boerboom, B. L. Schram, and J. Kistemaker, J. Chem. Phys. **44**, 4640 (1966).

[20] H. Chatham, D. Hils, R. Robertson, and A. Gallagher, J. Chem. Phys. **81**, 1770 (1984).

[21] O. J. Orient and S. K. Srivastava, J. Phys. B: At. Mol. Opt. Phys. **20**, 3923 (1987).

[22] H. C. Straub, D. Lin, B. G. Lindsay, K. A. Smith, and R. F. Stebbings, J. Chem. Phys. **106**, 4430 (1997).

[23] C. Tian and C. R. Vidal, J. Phys. B: At. Mol. Opt. Phys. **31**, 895 (1998).

[24] M. D. Ward, S. J. King, and S. D. Price, J. Chem. Phys. **134**, 024308 (2011).

[25] R. Browning and H. B. Gilbody, J. Phys. B: At. Mol. Opt. Phys. **1**, 1149 (1968).

[26] I. Ben-Itzhak, K. D. Carnes, D. T. Johnson, P. J. Norris, and O. L. Weaver, Phys. Rev. A **49**, 881 (1994).

[27] H. Knudsen, U. Mikkelsen, K. Paludan, K. Kirsebom, S. P. Møller, E. Uggerhøj, J. Slevin, M. Charlton, and E. Morenzoni, J. Phys. B: At. Mol. Opt. Phys. **28**, 3569 (1995).

[28] H. Luna, E. G. Cavalcanti, J. Nickles, G. M. Sigaud, and E. C. Montenegro, J. Phys. B: At. Mol. Opt. Phys. **36**, 4717 (2003).

[29] L. Gulyás, I. Tóth, and L. Nagy, J. Phys. B: At. Mol. Opt. Phys. **46**, 075201 (2013).

[30] C. C. Montanari and J. E. Miraglia, J. Phys. B: At. Mol. Opt. Phys. **47**, 015201 (2014).

[31] A. Salehzadeh and T. Kirchner, Eur. Phys. J. D **71**, 66 (2017).

[32] J. H. McGuire, *Electron Correlation Dynamics in Atomic Collisions* (Cambridge University Press, Cambridge, England, 1997).

[33] J. H. McGuire, Phys. Rev. Lett. **49**, 1153 (1982).

[34] J. H. McGuire, Phys. Rev. A **36**, 1114 (1987).

[35] A. K. Edwards, R. M. Wood, J. L. Davis, and R. L. Ezell, Phys. Rev. A **42**, 1367 (1990).

[36] A. K. Edwards, R. M. Wood, J. L. Davis, and R. L. Ezell, Phys. Rev. A **44**, 797 (1991).

[37] L. Nagy, J. H. McGuire, L. Végh, B. Sulik, and N. Stolterfoht, J. Phys. B: At. Mol. Opt. Phys. **30**, 1939 (1997).

[38] D. Fischer, R. Moshammer, A. Dorn, J. R. Crespo López-Urrutia, B. Feuerstein, C. Höhr, C. D. Schröter, S. Hagmann, H. Kollmus, R. Mann, B. Bapat, and J. Ullrich, Phys. Rev. Lett. **90**, 243201 (2003).

[39] T. Kirchner and H. Knudsen, J. Phys. B: At. Mol. Opt. Phys. **44**, 122001 (2011).

[40] W. Wolff, H. Luna, A. C. F. Santos, E. C. Montenegro, R. D. DuBois, C. C. Montanari, and J. E. Miraglia, Phys. Rev. A **84**, 042704 (2011).

[41] Natalia Ferreira, L. Sigaud, V. L. B. de Jesus, A. B. Rocha, L. H. Coutinho, and E. C. Montenegro, Phys. Rev. A **86**, 012702 (2012).

[42] Natalia Ferreira, L. Sigaud, and E. C. Montenegro, J. Phys.: Conf. Ser. **488**, 012042 (2014).

[43] L. Sigaud, Natalia Ferreira, L. H. Coutinho, V. L. B. de Jesus, and E. C. Montenegro, J. Phys. B: At. Mol. Opt. Phys. **45**, 215203 (2012).

[44] L. Sigaud, V. L. B. de Jesus, Natalia Ferreira, and E. C. Montenegro, Rev. Sci. Instrum. **87**, 083112 (2016).

[45] A. C. Cameron and F. A. G. Windmeijer, J. Econometrics **77**, 329 (1997).

[46] W. Wolff, I. J. de Souza, A. C. Tavares, G. F. S. de Oliveira, and H. Luna, Rev. Sci. Instrum. **83**, 123107 (2012).

[47] A. C. Tavares, H. Luna, W. Wolff, and E. C. Montenegro, Phys. Rev. A **92**, 032714 (2015).

[48] H. Luna, W. Wolff, E. C. Montenegro, A. C. Tavares, H. J. Lüdde, G. Schenk, M. Horbatsch, and T. Kirchner, Phys. Rev. A **93**, 052705 (2016).

[49] M. E. Rudd, R. D. DuBois, L. H. Toburen, C. A. Ratcliffe, and T. V. Goffe, Phys. Rev. A **28**, 3244 (1983).

[50] E. C. Montenegro, A. C. Tavares, H. Luna, and W. Wolff, J. Phys: Conf. Ser. **635**, 012019 (2015).

[51] E. C. Montenegro and G. M. Sigaud, J. Phys. B: At. Mol. Opt. Phys. **18**, 299 (1985).

[52] M. O. Krause, J. Phys. Chem. Ref. Data **8**, 307 (1979).

[53] Y. C. Yu, M. R. McNeir, D. L. Weathers, J. L. Duggan, F. D. McDaniel, and G. Lapicki, Phys. Rev. A **44**, 5702 (1991).

[54] E. C. Montenegro, G. M. Sigaud, and R. D. DuBois, Phys. Rev. A **87**, 012706 (2013).

[55] M. M. Sant'Anna, E. C. Montenegro, and J. H. McGuire, Phys. Rev. A **58**, 2148 (1998).

[56] C. C. Montanari and J. E. Miraglia, J. Phys. B: At. Mol. Opt. Phys. **45**, 105201 (2012).